View metadata, citation and similar papers at core.ac.uk
brought to you by CORE
provided by The University of Utah: J. Willard Marriott Digital Library

Mid- to long-wavelength infrared surface plasmon properties in doped zinc oxides

Justin W. Cleary[*a], Michael Snure [a], Kevin D. Leedy[a], David C. Look[b,c], Kurt Eyink[d], and Ashutosh Tiwari[e]

[a]Air Force Research Laboratory, Sensors Directorate, Wright Patterson AFB OH 45433
[b]Wyle Laboratories, Inc, Dayton, OH 45431
[c]Semiconductor Research Center, Wright State University, Dayton, OH 45435
[d]Air Force Research Laboratory, Materials Directorate, Wright Patterson AFB OH 45433
[e]Department of Materials Science and Engineering,University of Utah, Salt Lake City, UT 84112

ABSTRACT

This work investigates properties of surface plasmons on doped metal oxides in the 2-20 μm wavelength regime. By varying the stoichiometry in pulse laser deposited Ga and Al doped ZnO, the plasmonic properties can be controlled via a fluctuating free carrier concentration. This deterministic approach may enable one to develop the most appropriate stoichometry of ZnAlO and ZnGaO in regards to specific plasmonic applications for particular IR wavelengths. Presented are theoretical and experimental investigations pertaining to ZnAlO and ZnGaO as surface plasmon host materials. Samples are fabricated via pulsed laser deposition and characterized by infrared ellipsometry and Hall-effect measurements. Complex permittivity spectra are presented, as well as plasmon properties such as the field propagation lengths and penetration depths, in the infrared range of interest. Drude considerations are utilized to determine how the optical properties may change with doping. Finite element simulations verify these plasmonic properties. These materials not only offer potential use as IR plasmon hosts for sensor applications, but also offer new integrated device possibilities due to stoichiometric control of electrical and optical properties.

Keywords: plasmonics, infrared, sensors, waveguides, zinc oxides

1. INTRODUCTION

Surface plasmon polaritons (SPPs) are a means of current real-time, label-free biosensing [**1-3]** with current commercial surface plasmon resonance (SPR) biosensors being based in the visible or near-infrared wavelength regimes. Mid- to long-wave infrared SPR based biosensors would take advantage of the characteristic vibrational modes of biomolecules in this wavelength regime potentially giving increased sensitivity. SPPs also have potential in the development of mid- to long-wave infrared plasmonic waveguides or even hybrid dielectric/plasmonic subsystems [**4**] that could lead towards "plasmonic circuit" integration. While novel on-chip infrared plasmonic sensor designs have been investigated [**5-6**], work remains on the optimization and investigation of properties of the plasmonic hosts to be used.

The investigation of alternative plasmonic materials has recently been expanded upon [**7-10**] due to the large losses expected using noble metals as plasmon hosts and the drive to better enable fabrication of on-chip systems using standard techniques. Alternative hosts for plasmonics that have been investigated in the mid- to long-wave infrared includes highly doped-Si [**12-16**], metal silicides [**12, 14**], GeSn alloys [**4**], doped InAs [**17**], and the semimetal antimony [**18**]. Aluminum and gallium doped zinc oxides [**8, 10-11**] have been proposed as possible low-loss plasmonic materials in the near-IR. ZnO work has demonstrated largely fluctuating free carrier concentration, as well as mobility,

Optical Materials and Biomaterials in Security and Defence Systems Technology IX, edited by Roberto Zamboni, François Kajzar, Attila A. Szep, Proc. of SPIE Vol. 8545 854504 · © 2012 SPIE · CCC code: 0277-786/12/$18 · doi: 10.1117/12.974619

Downloaded From: http://spiedigitallibrary.org/ on 04/17/2013 Terms of Use: http://spiedl.org/terms

[**10, 19-21**] with slight changes in fabrication techniques and stoichiometry. These material properties ultimately are responsible in determining SPP properties such as propagation length and penetration depth, which are important in the aforementioned applications. Doped ZnO then has potential and should be considered for a novel class of broadly tunable plasmonic host materials.

Investigated here are plasmonic properties on doped zinc oxides in 2-20 μm infrared regime. Presented are theoretical and experimental investigations pertaining to ZnAlO and ZnGaO as surface plasmon host materials. Samples are fabricated via pulsed laser deposition and characterized by infrared ellipsometry and Hall-effect measurements. Complex permittivity spectra are presented, as well as plasmon properties such as the SPP propagation lengths and penetration depth. Drude considerations are utilized to determine how the optical properties may change with doping. Finite element simulations are utilized to verify these plasmonic properties.

2. THEORETICAL CONSIDERATIONS

Surface plasmon polaritons are bound electromagnetic waves that propagate along the interface between a dielectric and a conductor. The properties of SPPs can be determined from the wavelength-dependent complex optical constants of the dielectric and conducting regions. In order to determine plasmon properties, particular Drude parameters are necessary which themselves require knowledge of the carrier mobility, μ, and effective mass, *m**. Models to determine these parameters as a function of free carrier concentration exist for Ga doped ZnO [**21**] and in general apply to other doped ZnO's. Calculations of mobility in this work assume that the ratio of the number of acceptors to the number of donors is 0.2, which is a reasonable value for doped zinc oxides fabricated using typical PLD techniques.

Drude calculations of the complex permittivity are based the plasma frequency, ω_p, the relaxation frequency, ω_τ, which is the inverse of the relaxation time, $1/\tau$, and the high frequency dielectric constant, ε_∞. For lack of better knowledge, ε_∞ is taken to be 3.72 [**22**]. ω_p and ω_τ are determined by

$$\omega_p = \frac{2\pi c}{\lambda_p} = \sqrt{\frac{Ne^2}{m^* \varepsilon_\infty \varepsilon_o}}, \tag{1}$$

and

$$\omega_\tau = \frac{1}{\tau} = \frac{e}{\mu m^*}. \tag{2}$$

where λ_p is the plasmon wavelength, e is the electron charge, N is the free carrier concentration, and ε_o is the permittivity of free space. The complex permittivity is then determined by [**23**]

$$\varepsilon = \varepsilon' + \varepsilon'' = \varepsilon_\infty \left[1 - \frac{{\omega_p}^2}{\omega^2 + i\omega\omega_\tau} \right]. \tag{3}$$

Film characteristics to be determined directly from the above Drude parameters and optical constants are the optical skin depth (1/e optical field decay length) and the resistivity. The optical skin depth, δ, is found by

$$\delta = \frac{c}{\omega \, \mathrm{Im}\sqrt{\varepsilon}}, \tag{4}$$

and the resistivity, ρ, is found by

$$\rho = \frac{\omega_\tau}{\varepsilon_\infty \varepsilon_o \omega_p^2}. \tag{5}$$

Downloaded From: http://spiedigitallibrary.org/ on 04/17/2013 Terms of Use: http://spiedl.org/terms

The usefulness of any plasmonic materials or devices in potential applications is typically determined by the plasmonic penetration depth, a measure of mode confinement, and propagation length. First the complex SPP wavevector along the interface is found according to [**24**]

$$K_{SPP} = \frac{\omega}{c}\sqrt{\frac{\varepsilon_d\,\varepsilon_c}{\varepsilon_d + \varepsilon_c}}\,. \tag{6}$$

Here ε_d and ε_c are the complex permittivities of the dielectric and conductor, respectively. Then the 1/e plasmon intensity propagation length, 1/2 of the electric field propagation length, is determined by [**24**]

$$L_x = \frac{1}{2\mathrm{Im}\left(K_{SPP}(\omega)\right)}, \tag{7}$$

while the 1/e SPP field penetration depth into the dielectric or conductor can be determined by [**24**]

$$L_{d,c} = \left[\frac{\omega}{c}\mathrm{Im}\sqrt{\frac{\varepsilon^2{}_{d,c}}{\varepsilon_d + \varepsilon_c}}\right]^{-1}. \tag{8}$$

Finally, the coupling condition [**24**] between an electromagnetic wave, which is incident on the conducting grating from the dielectric at an angle θ from normal incidence, and an SPP is given by

$$\sin(\theta) + \frac{m\lambda}{p} = \pm\frac{c}{\omega}\mathrm{Re}[K_{SPP}]\,, \tag{9}$$

where p is the grating period, m is an integer of either sign, and λ is the excitation wavelength.

3. EXPERIMENTAL

ZnO films, doped with Al or Ga, characterized in this work were deposited on sapphire substrates via pulse laser deposition (PLD) using a KrF excimer laser. Films with compositions of $Zn_{0.995}Al_{0.005}O$ and $Zn_{0.982}Ga_{0.018}O$ were deposited under vacuum from ZnO targets with 0.6 wt.% Al_2O_3 and 1.2 wt.% Ga_2O_3 respectively Ref. [**20**] and Refs. [**19**]. A third film, $Zn_{0.974}Ga_{0.026}O$, was deposited in pure argon from a ZnO target with 3 wt.% Ga_2O_3, with this method having been investigated recently for fabrication of highly conductive ZnO [**21, 25**]. Film composition in all cases are nominal and are determined from donor concentrations assuming all donors were contributed from Al or Ga doping. [**26**].

The films were characterized via Hall-effect, ellipsometry, and profilometry measurements. Film thicknesses were determined via profilometry. An Accent HL5500 Hall System was used to determine the resistivity, mobility and carrier concentration. The films were also characterized using a J.A. Woollam IR-VASE ellipsometer in the wavelength range of 1 - 30 μm. The raw ellipsometry data is used in WVASE software and fitted Drude parameters and film thicknesses are determined for each sample.

4. RESULTS AND ANALYSIS

Table 1 presents all measured values. The Hall-effect measurements determined the sheet resistance, R_s, sheet charge density, N_s, and mobility while the profilometry revealed film thickness. The infrared ellipsometry data was fitted to determine the film thickness and Drude parameters ε_∞, ω_p, and ω_τ. The high frequency dielectric constants were allowed to vary in the fitting due to lack of knowledge of the Al or Ga doping effects. The profilometry and ellipsometry measurements confirm the order of magnitude of the film thicknesses although there may be variations in the film thickness. For our purposes, the thicknesses determined by ellipsometry will be used in further analysis since this measurement also resulted in the determination of optical constants at the same spot. N and ρ are found then by dividing N_s and multiplying R_s by the ellipsometry film thickness respectively. It must be noted the Hall-effect measurements

Downloaded From: http://spiedigitallibrary.org/ on 04/17/2013 Terms of Use: http://spiedl.org/terms

determine an average sheet charge density across the film which is used to determine *N* with a localized ellipsometry determined thickness. In the future, spatially periodic ellipsometry measurements can aid in determining film uniformity.

Figure 1 shows λ_p, μ, and ρ as a function of *N* for both the fabricated doped zinc oxides and calculations for a family of Ga-doped zinc oxides. All measured values were obtained by ellipsometry and Hall-effect measurements (Table 1). The Drude λ_p are then calculated using Eq. 1, while ρ is calculated using Eqs. 1, 2 and 5. The λ_p plot reveals that for plasmonics in the range of 6-12 μm, an *N* greater than ~$5x10^{19}$ cm^{-3} is necessary. μ is shown to decrease with increasing doping as expected due to an increasing number of scattering centers. The agreement of the mobility calculations and measured values indicates that the assumed ratio of the number of acceptor to the number of donors of 0.2 is accurate to within ± 25 % for the samples investigated [**21**]. ρ also decreases with increasing doping as expected for a material becoming more metal-like. In general, the measured values and the calculated Drude values agree even though one of the samples contains a different dopant (Al). Differences between the Drude and the measured values may lie in ε_∞, and the functions used for m^* and μ. It is noted that the mobility model used [**21**] was intended for *N* greater than ~$1x10^{20}$ cm^{-3}, although the Drude results shown here for lower carrier concentrations appear reasonable.

Table 1: Measured and fitted values for doped ZnO samples.

	Hall-effect			**Profilometer**	**Ellipsometer**			
	N_s	μ	R_s	thickness	thickness	ω_p	ω_τ	ε_∞
	[cm^{-2}]	[cm^2/Vs]	[Ω/Sq.]	[nm]	[nm]	[cm^{-1}]	[cm^{-1}]	Unit-less
$Zn_{0.995}Al_{0.005}O$	2.93e15	28.6	74.4	~200	155	3308	1041	4.02
$Zn_{0.982}Ga_{0.018}O$	1.26e16	22.0	22.5	~300	412	4295	1097	3.28
$Zn_{0.974}Ga_{0.026}O$	1.77e16	27.4	12.9	178	165	7192	724	3.19

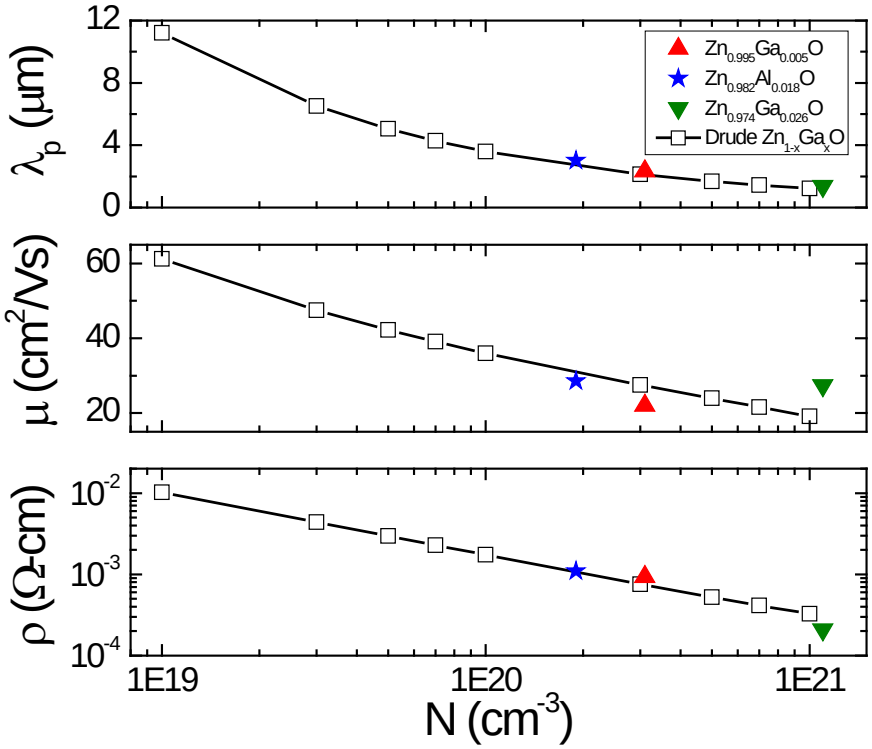

Figure 1: Plasmon wavelength (top), mobility (center), and resistivity (bottom) as a function of free carrier concentration. The solid symbols are determined from measurements and the open symbols are calculated.

Downloaded From: http://spiedigitallibrary.org/ on 04/17/2013 Terms of Use: http://spiedl.org/terms

The wavelength at which plasmonics becomes possible is the wavelength at which the real part of the permittivity crosses zero. Although this condition is not absolute [**18, 27**], this zero crossing, not exactly λ_p as can be seen by Eq. 3, remains a good metric for the low wavelength limit of plasmonic materials. Figure 2 presents the permittivity spectra obtained by the ellipsometry fitting for the three measured samples, and Drude calculations using Eq. 3. The real part, of the permittivity, ε', for the $Zn_{0.995}Al_{0.005}O$, $Zn_{0.982}Ga_{0.018}O$, and $Zn_{0.974}Ga_{0.026}O$ films goes negative at 3.2, 2.4, and 1.4 μm respectively. The imaginary part of the permittivity, ε'', increases with wavelength as expected for a Drude material. As noted earlier, all parameters, such as ε_∞, m^* and μ, used in the Drude calculations may have subtle differences from values determined from the films. The calculated values are intended to give a representation of the general trends.

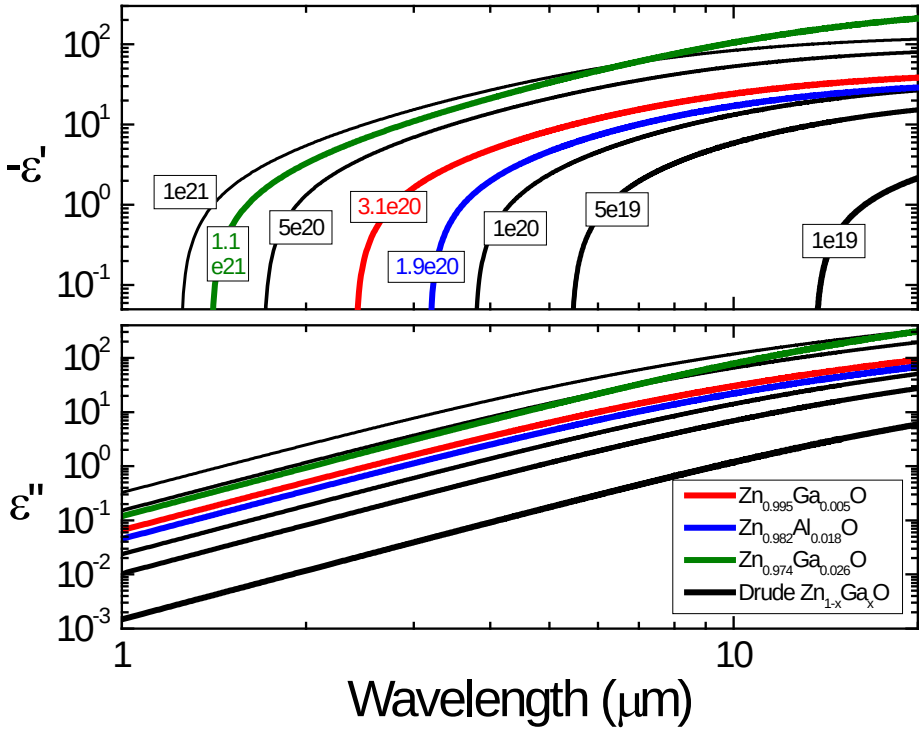

Figure 2: Negative real part (top) and imaginary part (bottom) of the permittivity spectra. The colored lines are determined from measurements and the black lines are calculated. The boxed numbers on the lines indicate either the *N* determined from Hall-effect measurements or the *N* used in calculations. *N* values are in units of cm^{-3}.

Figure 3 presents the optical skin depths, determined by Eq. 4 using the fitted Drude parameters (Table 1) of the three measured doped zinc oxides. At a wavelength of 10 μm, the optical skin depth of the measured $Zn_{0.974}Ga_{0.026}O$ is roughly half of that of the measured $Zn_{0.982}Ga_{0.018}O$ which is expected since the material is becoming increasingly metal-like with the increasing number of free carriers. Certain plasmonic applications may require the conducting material to allow some incident light penetration, although in many cases, such as the in-coupling of surface plasmons with a 2-D grating coupler, the film should be thicker than the skin depth to allow zero transmission. The $Zn_{0.974}Ga_{0.026}O$ sample, with $\delta < 150$ nm over roughly the 2.5-12 μm wavelength range, would require film thicknesses of at least 300-450 nm (2-3x the skin depth) to be sufficient for plasmonic applications that required zero transmission. These thicknesses are achievable using the fabrication techniques discussed here. Also shown for comparison in Fig. 3 are dashed lines which represent the film thicknesses determined by ellipsometry. In each case, the film thickness is smaller than or nearly the same as the optical skin depth in the mid- to long-wave infrared. This led to the raw ellipsometry output being less Drude-like at the long-wavelength side of the ellipsometer measurements. This is overcome by using the WVASE fitting software with the inclusion of the sapphire substrates to determine the parameters for the specific films themselves.

Downloaded From: http://spiedigitallibrary.org/ on 04/17/2013 Terms of Use: http://spiedl.org/terms

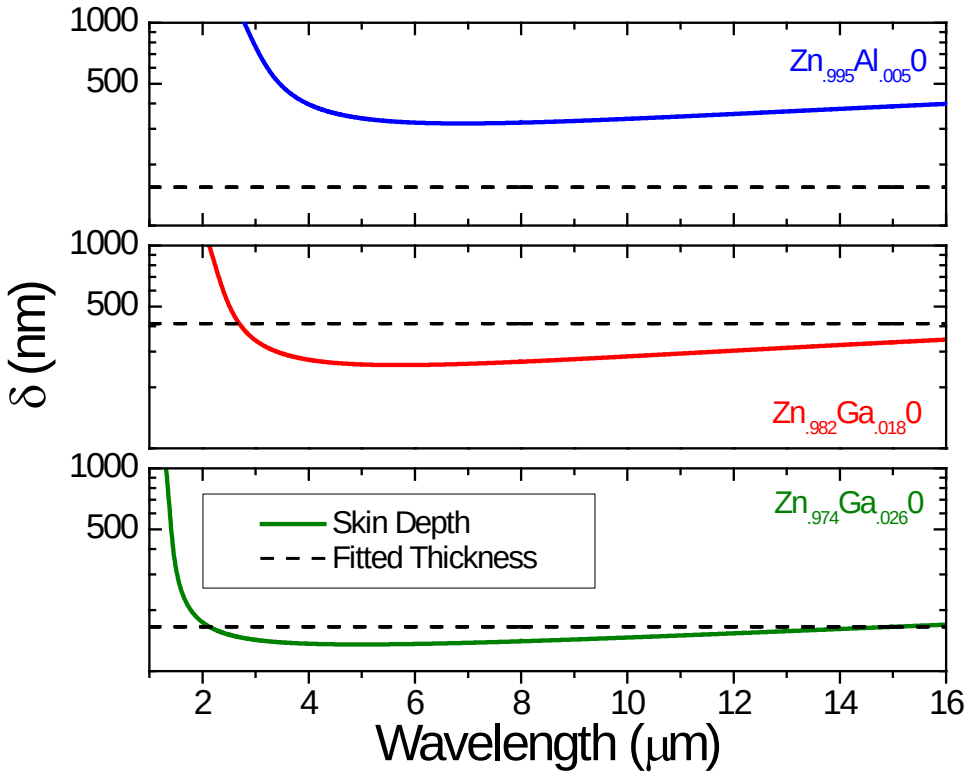

Figure 3: The optical skin depths (colored lines) and film thicknesses (dashed lines) determined from measurements.

Figure 4 presents the plasmon intensity propagation length (upper) and field penetration depth (lower) into both the conductor (L_c) and into air (L_d) as a function of wavelength. Values calculated via the ellipsometry data are colored, while the black lines are based on Drude theory. In all cases, the values are determined from the permittivity (Figure 2) and Eqs. 6-8. Only the range for which $\varepsilon' < 0$ is plotted for each material. In all cases, L_x increases with increasing wavelength. The penetration depth into air, L_d, is less than the wavelength for $\lambda < 10.8$, 9.1, and 5.2 μm for the investigated $Zn_{0.995}Al_{0.005}O$, $Zn_{0.982}Ga_{0.018}O$, and $Zn_{0.974}Ga_{0.026}O$ respectively. These regimes may be useful in sensing applications where propagation length is unimportant and the smallest mode confinement may be critical for sensitivity purposes. For the three respective samples, the L_x is greater than the wavelength for $\lambda > 4.7$, 3.7, and 2.0 μm which is important to note for possible waveguide or other applications.

Finite element method (FEM) simulations were completed using the RF package of COMSOL Multiphysics. These results support the interpretation of resonant excitation of SPPs and associated properties on the investigated doped zinc oxides. The 2-D grating, which has been shown to in-couple incident long-wavelength infrared irradiation to SPPs and similar bound waves [**16, 18, 28**], is used here to investigate the relevant SPP properties. Figure 5 presents contour plots of the electric field distribution in the case of an incident polarized field with a specified λ and θ, on a 2-D doped zinc oxide lamellar grating of 20 μm period, 2 μm height, and 50% duty cycle. The angle of incidence in this case is 24° from the normal as required by Eq. 9 for the excitation of the first order SPP mode. The contour scales in each image were changed to clearly illustrate the SPP properties under investigation. Changes in the field strengths at the end of the in-coupler grating are not emphasized since the change in in-coupling between different materials and possible immediate out-coupling are not well understood.

Downloaded From: http://spiedigitallibrary.org/ on 04/17/2013 Terms of Use: http://spiedl.org/terms

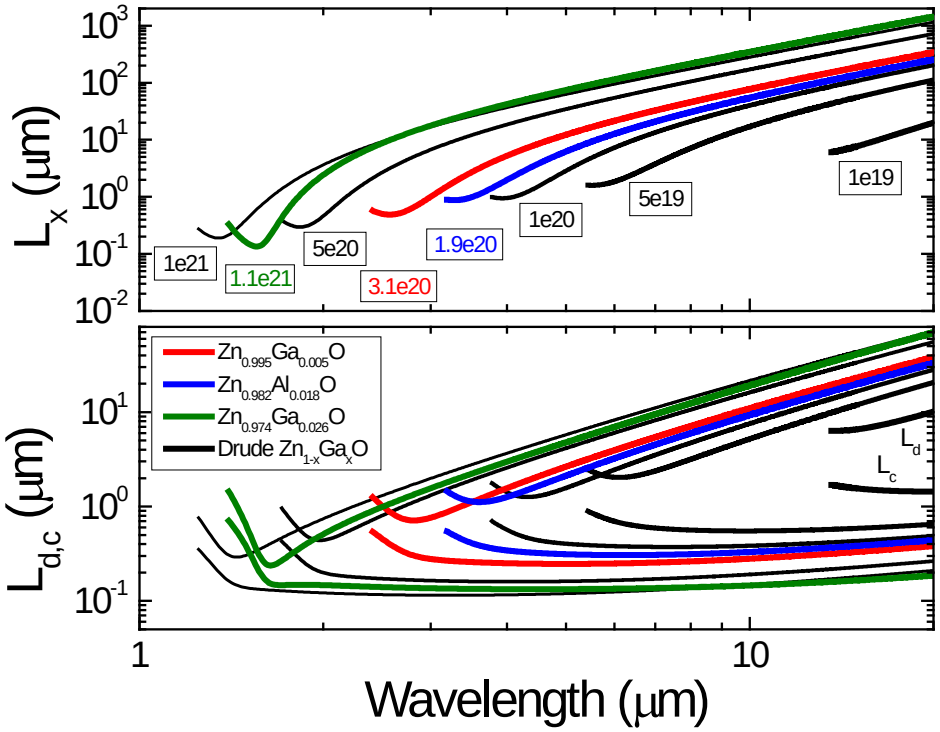

Figure 4: SPP intensity propagation length (top) and field penetration depth (bottom). The colored lines are determined from measurements and the black lines are calculated. The boxed numbers on the lines indicate either the *N* determined from Hall-effect measurements or the *N* used in calculations. *N* values are in units of cm^{-3}. In the bottom curve, the upper set of lines give L_d with the dielectric being air, while the lower set of lines give L_c.

Figure 5 (left) present a large scale image of the square of the component of electric field normal to the surface, E_n^2. The dimension of the x-axis is roughly 500 μm, while the y-axis is roughly 330 μm. The left side of the images depicts the ending of the in-coupling grating with reflected light and possible out-coupled SPP fields leaving the plane. Since the SPP fields decay exponentially along the interface [**24**], and E^2 is proportional to intensity, the 1/e propagation length of the pictured E_n^2 is representative of the intensity propagation length. The propagation length in the simulation is determined to be 70, 115, and 370 μm for the $Zn_{0.995}Al_{0.005}O$, $Zn_{0.982}Ga_{0.018}O$, and $Zn_{0.974}Ga_{0.026}O$ films respectively. These values correspond well with those calculated analytically (Figure 4) of 84, 115, 505 μm. There is a 36% difference between the analytical and simulated value for the largest Ga-doped sample, although constraints on the x-y simulation size may have influenced the shorter propagation length.

Figure 5 (right) presents a magnified snapshot of the normal field component, E_n. The dimension of the x-axis is roughly 55 μm, while the y-axis is roughly 40 μm. The 1/e penetration depth into the dielectric (air) in the simulation is determined to be 14, 15, and 29 μm for the $Zn_{0.995}Al_{0.005}O$, $Zn_{0.982}Ga_{0.018}O$, and $Zn_{0.974}Ga_{0.026}O$ films respectively. These values correspond well with those calculated analytically (Figure 4) of 13, 15, 27 μm with the respective analytical and simulations values being within 8%. The SPP fields are not observed in the conducting region which is expected since the corresponding penetration depths are (Figure 4) 150, 300, and 350 nm respectively for the $Zn_{0.995}Al_{0.005}O$, $Zn_{0.982}Ga_{0.018}O$, and $Zn_{0.974}Ga_{0.026}O$ films.

Downloaded From: http://spiedigitallibrary.org/ on 04/17/2013 Terms of Use: http://spiedl.org/terms

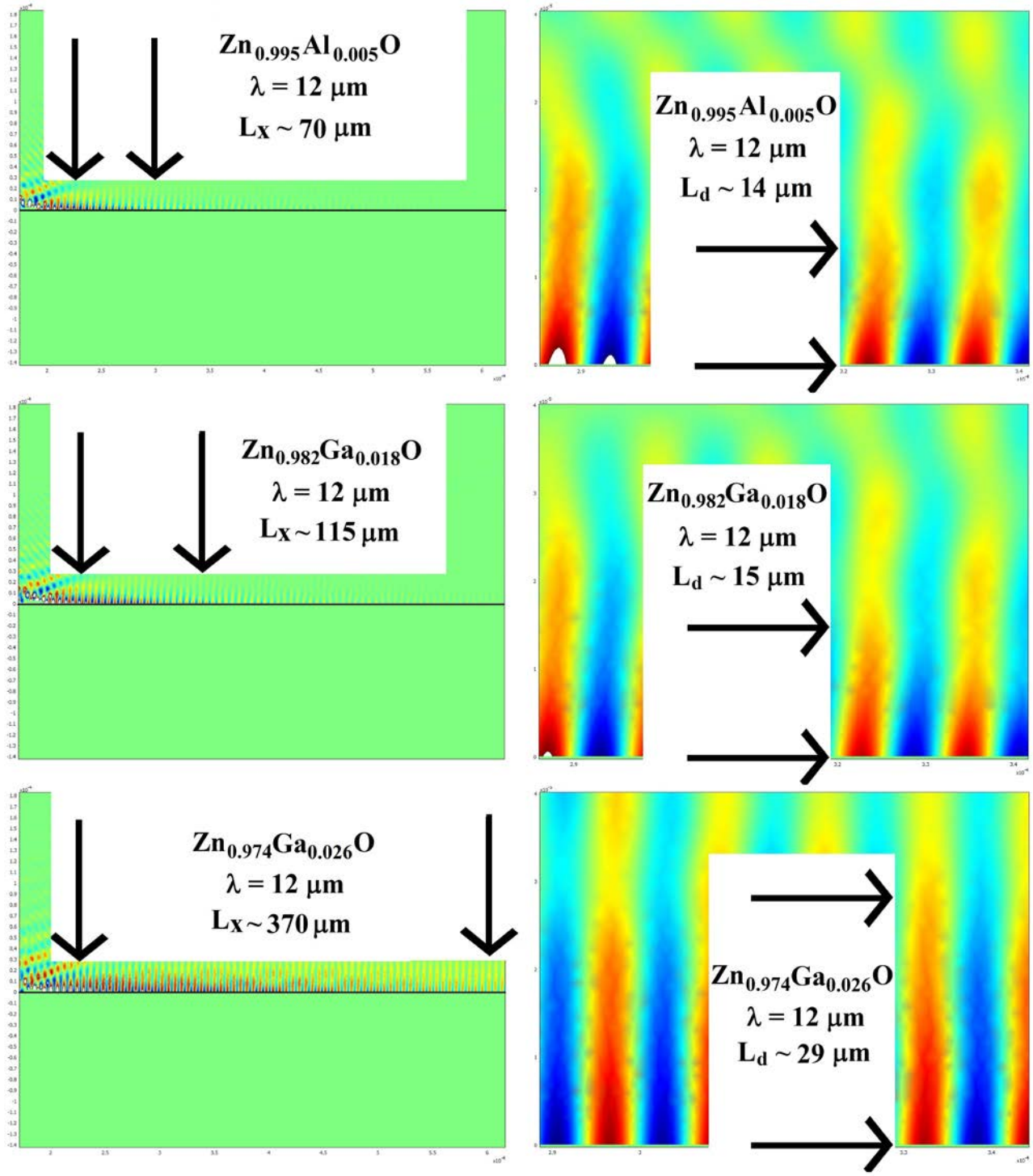

Figure 5: Spatial electric field intensity demonstrating SPP propagation length, L_x, (left) and spatial electric field demonstrating SPP penetration depth, L_d, (right). The SPP modes are in-coupled using a 2-D grating coupler with a 20 μm period and 50% duty cycle. The incident polarized plane light with λ = 12 μm was 24° from the normal at the surface, which gives the first order excitation. The solid black lines separate the upper dielectric (air) from the lower conducting regions.

Downloaded From: http://spiedigitallibrary.org/ on 04/17/2013 Terms of Use: http://spiedl.org/terms

Results presented in this work pertain to doped zinc oxides with a ratio of the number of acceptors to the number of donors assumed to be 0.2 for calculations with experimental data appearing to agree to within ± 25 % of this value. Recent works have strived to achieve highly conductive zinc oxides by eliminating acceptors [**21**], although the infrared plasmonics field may benefit from the broad range of electrical and optical properties found by these inclusions. To take a quick look, if the number of acceptors is modified to give a ratio, again N_a/N_d, between 0 – 0.4, the mobility falls in the range of 48-4.7 and 85-9 cm^2/Vs for $N = 10^{21}$ and 10^{20} cm^{-3} respectively [**21**]. While this has no effect on the Drude plasmon frequency if the effective number of free carriers remains the same (Eq. 1), the fluctuating mobility has an effect on ω_τ (Eq. 2). In this cases of relatively low mobility, or $N_a/N_d = 0.4$, ω_τ and ω_p become the same order of magnitude, which occurs occurs in general for decreasing N. These materials, with potentially tunable ω_τ and ω_p via fabrication techniques, may provide a useful basis for infrared plasmonics in applications where small penetration depths may be necessary (sensors) or where specific penetration depth vs. propagation lengths are desired (on-chip waveguiding). These fabrication tunable properties will be investigated more thoroughly in the future.

5. SUMMARY AND OUTLOOK

This paper described investigations of optical and electrical characterstics of Ga- and Al-doped zinc oxides and discussed possible plasmonic properties in the mid- to long-wavelength infrared. Ellipsometry measurements indicate that Ga-doped zinc oxides with free carrier concentrations on the order of 10^{21} cm^{-3} may enable plasmonics at wavelengths > 1.4 μm. The SPP penetration depth into air for this highly doped zinc oxide is sub-wavelength up to approximately 5 μm. At wavelengths beyond 5 μm, sub-wavelength SPP penetration depths are still achievable via lower doping as indicated here with Ga- and Al- doped ZnO with N~ 10^{20} cm^{-3}. The Ga-doped zinc oxides with free carrier concentrations ~ 10^{21} cm^{-3} also indicates that SPP intensity propagation lengths on the order hundreds of microns are possible in the mid- to long-wavelength IR with even 0.5 mm possible at wavelengths near 11 μm.

By varying the stoichiometry and fabrication techniques in pulse laser deposited Ga and Al doped ZnO, the plasmonic properties can be controlled via a fluctuating free carrier concentration and mobility. The deterministic approach for ZnAlO and ZnGaO has potential for tailoring plasmonic for applications in the 2-20 μm wavelength regime. These materials not only offer potential use as IR plasmon hosts, but also offer new integrated device possibilities due to stoichiometric control of electrical and optical properties. Future investigations should explore Ga- and Al-doping effects on the high frequency dielectric constant, the effects on vacancies on ω_τ and ω_p, which ultimately effect plasmonic properties.

ACKNOWLEDGMENTS

JWC would like to acknowledge support from the Air Force Office of Scientific Research (Program Manager Dr. Gernot Pomrenke) under contract number 12RY10COR. DCL would like acknowledge support also from Air Force Office of Scientific Research (Program Manager Dr. James Hwang) under grant number FA9550-10-1-0079. We also acknowledge Tim A. Cooper for Hall-effect measurements.

REFERENCES

[1] Homola, J., "Present and future of surface plasmon resonance biosensors," Anal. Bioanal. Chem. **377**, 528-539 (2003).
[2] Rich R. L. and Myszka, D. G., "Advances in surface plasmon resonance biosensor analysis," Curr. Opin. Biotech. **11**, 54-61 (2000).
[3] Zhao, J., Zhang, X., Yonzon, C. R., Haes, A. J. and Van Duyne, R. P., "Localized surface plasmon resonance biosensors," Nanomedicine **1**, 219-228 (2006).

Downloaded From: http://spiedigitallibrary.org/ on 04/17/2013 Terms of Use: http://spiedl.org/terms

[4] Soref, R., Hendrickson, J., and Cleary, J. W., "Mid- to long-wavelength infrared plasmon-photonics using heavily doped n-Ge/Ge and n-GeSn/GeSn heterostructures," Opt. Express, **20**, 3814-3824 (2012).
[5] Fredricksen, C. J., Cleary, J. W. Buchwald, W. R., Figueiredo, P., Khalilzadeh-Rezaie, F., Medhi, G., Rezadad, I., Shahzad, M., Yesiltas, M., Nath, J., Boroumand, J., and Peale, R. E., "Planar integrated plasmonic mid-IR spectrometer," Proc. SPIE 8353-33 (2012).
[6] Oh, G., Lee, T., Kim, H., Kim, D. G., and Choi, Y., "Design of ultra-sensitive biosensor applying surface plasmon resonance to a triangular resonator," Opt. Express **20**, 19067-19074 (2012).
[7] Murray, A. W., and Barnes, W. L., "Plasmonic materials," Adv. Mater. **19**, 3771-3782 (2007).
[8] West, R. R., Ishii, S., Naik, G., Emani, N., Shalaev, V. M., and Boltasseva, A., "Searching for better plasmonic materials," Laser & Photon. Rev. **4**, 795-808 (2010).
[9] Boltasseva, A., and Atwater, H. A., "Low-loss plasmonic metamaterials," Science **331**, 290-291 (2011).
[10] Naik, G., and Boltasseva, A., "Plasmonics and metamaterials" looking beyong gold and silver," SPIE Newsroom Optoelectronics and Communicatins, 30 Jan. 2012.
[11] Naik, G., Kim, J., and Boltasseva, A., "Oxides and nitrides as alterative plasmonic materials in the optical range," Opt. Mat. Express **1**, 1090-1099 (2011).
[12] Soref, R., Peale, R. E., and Buchwald, W., "Longwave plasmonics on doped silicon and silicides," Opt. Express **16**, 6507-6514 (2008).
[13] Chen, Y., "Development of mid-infrared surface plasmon resonance-based sensors with highly-doped silicon for biomedical and chemical applications," Opt. Express **17**, 3130-3140 (2009).
[14] Cleary, J. W., Peale, R. E., Shelton, D. J., Boreman, G. D., Smith, C. W., Ishigami, M., Soref, R., Drehman, A., and Buchwald, W.R., "IR permittivities for silicides and doped silicon," J. Opt. Soc. Am. B **27**, 730-734 (2010).
[15] Ginn, J. C., Jarecki, Jr., R. L., Shaner, E. A., and Davids, R. S., "Infrared plasmons on heavily-doped silicon," J.Appl. Phys. **110**, 043110 (2011).
[16] Shahzad, M., Medhi, G., Peale, R. E., Buchwald, W. R., Cleary, J. W., Soref, R., Boreman, G. D., and Edwards, O., "Infrared surface plasmons on heavily doped silicon," J.Appl. Phys., **110**, 123105 (2011).
[17] Law, S., Adams, D. C., Taylor, A. M., and Wasserman, D., "Mid-infrared designer metals," Opt. Express **20**, 12155-12165 (2012).
[18] Cleary, J. W., Medhi, G., Shahzad, M., Rezadad, I., Maukonen, D., Peale, R. E., Boreman, G. D., Wentzell, S., and Buchwald, W. R., "Infrared surface polaritons on antimony," Opt. Express **20**, 2693-2705 (2012).
[19] Snure, M., and Tiwari, A., "Structural, electrical, and optical characterizations of epitaxial $Zn_{1-x}Ga_xO$ films grown on sapphire (0001) substrate," J. Appl. Phys. **101**, 124912 (2007).
[20] Snure, M., Toledo, D., Slusser, P., and Tiwari, A., "Conduction in degenerately-doped $Zn_{1-x}Al_xO$ thin films," in [GaN and ZnO-based materials and devices], Springer-Verlag, Berlin Heidelberg, 349-360 (2012).
[21] Look, D. C., and Leedy, K. D., "Making highly conductive ZnO: creating donors and destroying acceptors," Proc. SPIE 826302 (2012).
[22] Madelung, O., [Semiconductors: Data Handbook 3rd edition], Springer, Berlin (2004).
[23] Yu, P. Y. and Cardona, M. [Fundamentals of Semiconductors], Springer, Berlin (1996).
[24] Raether, H. [Surface Plasmons on Smooth and Rough Surfaces and on Gratings] Springer, New York (1988).
[25] Scott, R.C., Leedy, K. D., Bayraktaroglu, B., Look, D.C., and Zhang, Y-H., "Highly conductive ZnO grown by pulsed laser deposition in pure Ar," Appl. Phys. Lett. **97**, 072113 (2010).
[26] Look, D. C., Leedy, K. D., Tomich, D. H., and Bayraktaroglu, B., "Mobility analysis of highly conducting thin films: Application to ZnO," Appl. Phys. Lett. **96**, 062102 (2010).
[27] Yang, F., Sambles, J. R., and Bradberry, G. W., "Long Range Surface Modes Supported By Thin Films," Phys. Rev. B **44**, 5855–5872 (1991).
[28] Cleary, J. W., Peale, R. E., and Buchwald, W. R., "Long-wave infrared surface plasmon grating coupler," Appl. Opt. **49**, 3102-3110 (2010).

Downloaded From: http://spiedigitallibrary.org/ on 04/17/2013 Terms of Use: http://spiedl.org/terms